Strategies for RANS/VMS-LES coupling

Gennaro Pagano, Simone Camarri, Maria Vittoria Salvetti, Bruno Koobus, Alain Dervieux

INSTITUT NATIONAL DE RECHERCHE EN INFORMATIQUE ET EN AUTOMATIQUE

Strategies for RANS/VMS-LES coupling

Gennaro Pagano, Simone Camarri, Maria Vittoria Salvetti, Bruno Koobus, Alain Dervieux

N° 5954

July 2006

Thème NUM

ISSN 0249-6399 ISRN INRIA/RR--5954--FR+ENG

Strategies for RANS/VMS-LES coupling

Gennaro Pagano*, Simone Camarri†, Maria Vittoria Salvetti‡, Bruno Koobus§, Alain Dervieux¶

Thème NUM — Systèmes numériques
Projet Smash

Rapport de recherche n° ???? — July 2006 — 43 pages

Abstract: A new hybrid RANS/LES approach is proposed. The key feature of this approach is a blending between two eddy-viscosities, one given by the $k-\varepsilon$ RANS model and the other by the Smagorinsky VMS-LES (variational multiscale LES) closure. The blending is set by a parameter θ: VMS-LES mode is active when $\theta = 0$, RANS mode if $\theta = 1$, a hybrid mode for $0 < \theta < 1$. The proposed hybrid model has been applied to the numerical simulation of the flow around a square cylinder at $Re_L = 22000$. Three different parameters (based on viscosity ratio, time ratio and length ratio) are tested. The results obtained with this new hybrid approach are compared with those obtained using the LNS approach for two different grid resolutions; comparisons with experimental data in the litterature are also provided. The sensitivity of the model to some setting parameters (the inflow value of the turbulent kinetic energy, k_0 and the parameter δ in the approximate wall treatment) is also analysed.

Key-words: Hybrid RANS/LES Turbulence Models, Variational Multiscale Approach (VMS), Limited Numerical Scales (LNS), Complex Geometries, Unstructured Grids.

* Dipl. Ingegneria Aerospaziale, Via Caruso,56126 Pisa (Italy)
† Dipl. Ingegneria Aerospaziale, Via Caruso,56126 Pisa (Italy)
‡ Dipl. Ingegneria Aerospaziale, Via Caruso,56126 Pisa (Italy)
§ Dept Mathématiques, Univ. Montpellier II, CC.051, 34095 Montpellier, France, and INRIA
¶ INRIA, 2004 Route des Lucioles, BP. 93, 06902 Sophia-Antipolis, France

Unité de recherche INRIA Sophia Antipolis
2004, route des Lucioles, BP 93, 06902 Sophia Antipolis Cedex (France)
Téléphone : +33 4 92 38 77 77 — Télécopie : +33 4 92 38 77 65

Stratégies de couplage RANS/VMS-LES

Résumé : Une nouvelle approche hybride RANS/LES (RANS: Reynolds Averaged Navier-Stokes/Navier-Stokes avec moyenne de Reynolds ; LES: Large Eddy Simulation/Simulation de grandes Structures) est appliquée à la simulation numérique de l'écoulement autour d'un cylindre carré. Le dispositif principal de cette approche est la fusion entre deux viscosités turbulentes, l'une donnée par le modèle RANS $k-\varepsilon$ et l'autre par une formulation VMS-LES (VMS: Variational Multiscale) basée sur la fermeture LES de Smagorinsky. La fusion entre les deux modèles est controlée par le paramètre θ : VMS-LES est appliqué là où $\theta = 0$, RANS là où $\theta = 1$, et un mode intermédiaire pour $0 < \theta < 1$. Trois paramètrages différents (basés sur le rapport de viscosité, le rapport de temps et le rapport de longueur) sont examinés. Les résultats obtenus avec cette nouvelle approche hybride sont comparés à ceux obtenus en utilisant l'approche LNS (Limited Numerical Scale) pour deux résolutions différentes de grille; des comparaisons avec les données expérimentales sont également proposées. La sensibilité du modèle à quelques paramètres de réglage (le niveau k_0 d'apport d'énergie cinétique turbulente et le paramètre δ dans le traitement approximatif des couches limites) est également analysée.

Mots-clés : Turbulence, Hybrides RANS/LES, Variational Multiscale, Limited Numerical Scales, géométries complexes, maillages non-structurés

1 Introduction

The Direct Numerical Simulation (DNS) of the Navier-Stokes equations is feasible only for low Reynolds numbers (Re) due to the necessary computational resources, which already become prohibitively large for $Re \simeq 10^4$. For this reason, turbulence modeling is a necessary step for the numerical simulation of flows of engineering interest. In this context, the most widely used approach for the simulation of high-Reynolds number turbulent flows is the one based on the Reynolds-Averaged Navier-Stokes equations (RANS). In the RANS approach, time averaging is applied to the Navier-Stokes equations and only the time-averaged flow is simulated. In this way a noticeable simplification of the problem is obtained, computational costs are drastically reduced and become almost independent of the Reynolds number when this is sufficiently large. However, RANS models usually have difficulties in providing accurate predictions for flows with massive separations, as for instance for the flow around bluff bodies, for which they are too dissipative to properly simulate 3D phenomena, yielding to significant discrepancies with respect to the experimental results.

An alternative approach is the Large-Eddy simulation (LES), in which a spatial filter is applied to the equations in order to get rid of small-scale turbulent fluctuations which are thus modeled, and the remaining flow scales are directly simulated. Since the dynamics of large scales is directly simulated and three-dimensionality and unsteadiness of the flow are naturally taken into account, the LES approach is generally more accurate, but also computationally more expensive, than the RANS one. Moreover, the cost of LES simulations increases as the flow Reynolds number is increased. Indeed, the grid has to be fine enough to resolve a significant part of the turbulent scales, and spatial resolution becomes particularly critical in the near-wall regions.

A new class of models has been recently proposed in the literature in which RANS and LES approaches are combined together in order to obtain simulations as accurate as in the LES case but at reasonable computational costs. Among different strategies of combining the two approaches, we consider here the *blending strategy*, in which RANS and LES are blended together in a continuous way throughout the computational domain. This approach leads to the so-called *universal models*.

Among the *universal models* described in the literature, the Detached Eddy Simulation (DES) has received the largest attention. This approach, first described in Ref. ([22]), is based on the one-equation Spalart-Allmaras RANS model, in which the length scale of the turbulent kinetic energy destruction term is modified to be the minimum one between the distance to the wall and a length proportional to the local grid resolution. Thus, in the near-wall region and with RANS-like grids the Spalart-Allmaras RANS model is used, while far from the wall the simulation switches to the LES mode with a one-equation SGS closure (SGS: sub-grid scale).

Another hybrid approach, the Limited Numerical Scale (LNS) one, has been recently proposed in Ref. [1]. In this approach, the blending parameter depends on the values of the eddy-viscosity given by a RANS model, μ_t, and of the SGS viscosity given by a LES closure, μ_s. In practice, the minimum of the two eddy-viscosities is used. This should ensure that, where the grid is fine enough to resolve a significant part of the turbulence scales, the model

works in the LES mode, while elsewhere the RANS closure is recovered. An example of validation of this hybrid model for the simulation of bluff-body flows is given in Ref. [7].

In the present work, a new strategy is proposed for blending RANS and LES approaches in a hybrid model. To this purpose, as proposed in Ref. [13], the flow variables are decomposed in a RANS part (i.e. the averaged flow field), a correction part that takes into account the turbulent large-scale fluctuations, and a third part made of the unresolved or SGS fluctuations. The basic idea of the proposed approach is to solve the RANS equations in the whole computational domain and to correct the obtained averaged flow field by adding, where the grid is adequately refined, the remaining resolved fluctuations. The equations governing the resolved fluctuations are derived from the RANS and LES equations. Instead of using a zonal approach, in which regions to be treated by a RANS or LES approach are a-priori defined, as in Ref. [13], a *universal* hybrid model is proposed here. To this aim, a blending function is introduced, θ, which smoothly varies between 0 and 1. The correction term which is added to the averaged flow field is thus damped by a factor $(1-\theta)$, obtaining a model which coincides with the RANS approach when $\theta = 1$ and recovers the LES approach in the limit of $\theta \to 0$. Three different definitions of the blending function θ are proposed, based on the ratios between (i) the two eddy viscosities, (ii) two characteristic length scales and (iii) two characteristic time scales given by the RANS and the LES models, respectively. The RANS model used in the proposed hybrid model is the standard $k-\varepsilon$ model Ref. [15], while for the LES part the Variational Multi-Scale approach (VMS) Ref. [11] is adopted. The VMS approach can be compared in terms of accuracy to the dynamic Smagorinsky model, but its computational cost is definitely lower and comparable to that of the simple Smagorinsky model, as shown in Ref. [12].

The proposed model has been implemented in a numerical solver (AERO) for the Navier-Stokes equations in the case of compressible flows and perfect Newtonian gases, based on a mixed finite-element/finite-volume scheme formulated for unstructured grids made of tetrahedral elements. Finite elements (P1 type) and finite volumes are used to treat the diffusive and convective fluxes, respectively. Concerning the VMS approach, the version proposed in Ref. [12] for compressible flows and for the particular numerical method employed in AERO has been used here.

Also the LNS approach has been implemented in AERO as described in details in Ref. [7], using the standard $k-\varepsilon$ model and the Smagorinky SGS model as the RANS and LES part, respectively.

The capabilities of both the LNS approach and the proposed hybrid approach have been appraised in the simulation of the flow around a square cylinder at a Reynolds number, based on the far-field velocity and on the side length of the cylinder, equal to $Re = 22000$. For this value of the Reynolds number, several experimental and numerical results are available in the literature (see, for instance, Ref. [16],[3],[2]). Different simulations have been carried out by varying the grid refinement, the inflow value of the turbulent kinetic energy and the free parameter δ in the approximate wall treatment used in AERO, which is based on the Reichardt wall-law Ref. [10]. In the case of the proposed model, all the three different

proposals for the blending function θ have been tested. Comparisons with experimental data and numerical results in the literature are also provided.

2 Hybrid RANS/LES coupling

The Navier-Stokes equations for compressible flows of (calorically and thermally) perfect Newtonian gases are considered here, written in conservative form in the following variables (using Einstein notation): density (ρ), momentum (ρu_i, $i = 1, 2, 3$) and total energy per unit volume ($E = \rho e + 1/2 \rho u_i u_i$, e being the internal energy).

As in Ref. [13], the following decomposition of the flow variables is adopted:

$$w_i = \underbrace{< w_i >}_{RANS} + \underbrace{w_i^c}_{correction} + {w_i}^{SGS}$$

where $< w_i >$ are the flow variables in RANS, obtained by applying an averaging operator to the Navier-Stokes equations, w_i^c are the remaining resolved fluctuations (i.e. $< w_i > + w_i^c$ are the flow variables in LES) and ${w_i}^{SGS}$ are the unresolved or SGS fluctuations.

If we write the Navier-Stokes equations in the following compact conservative form:

$$\frac{\partial \boldsymbol{W}}{\partial t} + \nabla \cdot F(\boldsymbol{W}) = 0$$

in which F represents both the viscous and the convective fluxes, for the averaged flow $\langle \boldsymbol{W} \rangle$ we get:

$$\frac{\partial \langle \boldsymbol{W} \rangle}{\partial t} + \nabla \cdot F(\langle \boldsymbol{W} \rangle) = -\tau^{RANS}(\langle \boldsymbol{W} \rangle) \tag{1}$$

where $\tau^{RANS}(\langle \boldsymbol{W} \rangle)$ is the closure term given by a RANS turbulence model.

As well known, by applying a filtering operator to the Navier-Stokes equations, the LES equations are obtained, which, in the previously introduced notations, can be written:

$$\frac{\partial \langle \boldsymbol{W} \rangle + \boldsymbol{W}^c}{\partial t} + \nabla \cdot F(\langle \boldsymbol{W} \rangle + \boldsymbol{W}^c) = -\tau^{LES}(\langle \boldsymbol{W} \rangle + \boldsymbol{W}^c) \tag{2}$$

where τ^{LES} is the SGS term.

An equation for the resolved fluctuations $\boldsymbol{W}^c$ can thus be derived as follows (see also Ref. [13]):

$$\frac{\partial \boldsymbol{W}^c}{\partial t} + \nabla \cdot F(\langle \boldsymbol{W} \rangle + \boldsymbol{W}^c) \; - \; \nabla \cdot F(\langle \boldsymbol{W} \rangle) = \tau^{RANS}(\langle \boldsymbol{W} \rangle) - \tau^{LES}(\langle \boldsymbol{W} \rangle + \boldsymbol{W}^c) \tag{3}$$

The basic idea of the proposed hybrid model is to solve Eq. (1) in the whole domain and to correct the obtained averaged flow by adding the remaining resolved fluctuations (computed through Eq. (3)), wherever the grid resolution is adequate for a LES. Instead of using a zonal approach as in Ref. [13], in which the regions where the additional fluctuations that must be computed are a-priori defined, we wish to construct a *universal* hybrid model. To this aim, we introduce a *blending function*, θ, smoothly varying between 0 and 1. When $\theta = 1$, no correction to $\langle \boldsymbol{W} \rangle$ is computed and, thus, the RANS approach is recovered. Conversely, wherever $\theta < 1$, additional resolved fluctuations are computed; in the limit of

$\theta \rightarrow 0$ we want to recover a full LES approach. The definition of the blending function is discussed in details in Sec. 2.1. Thus, wherever $\theta < 1$, we also solve the following equation for the fluctuations:

$$\begin{aligned} &\frac{\partial \boldsymbol{W}^c}{\partial t} + \nabla \cdot F(\langle \boldsymbol{W} \rangle + \boldsymbol{W}^c) - \nabla \cdot F(\langle \boldsymbol{W} \rangle) = \\ &(1-\theta)\left[\tau^{RANS}(\langle \boldsymbol{W} \rangle) - \tau^{LES}(\langle \boldsymbol{W} \rangle + \boldsymbol{W}^c)\right] \end{aligned} \tag{4}$$

Note that for $\theta \rightarrow 1$ the RANS limit is actually recovered; indeed, for $\theta = 1$ the right-hand side of Eq. (4) vanishes and, hence, a trivial solution is $\boldsymbol{W}^c = 0$. As required, for $\theta = 0$ Eq. (4) becomes identical to Eq. (3) and the remaining resolved fluctuations are added to the averaged flow; the model, thus, works in LES mode. For θ going from 1 to 0, i.e. when, following the definition of the blending function (see Sec. 2.1), the grid resolution is intermediate between one adequate for RANS and one adequate for LES, the righthandside term in Eq. (4) is damped through multiplication by $(1-\theta)$. Although it could seem rather arbitrary from a physical point of view, this is aimed to obtain a smooth transition between RANS and LES. More specifically, we wish to obtain a progressive addition of fluctuations when the grid resolution increases and the model switches from the RANS to the LES mode, in order to try to overcome the well known problems of existing universal hybrid models in the transition from RANS to LES, as, for instance, the "gray zones" in DES or the need of addition of synthetic turbulence in LNS Ref. [1].

Summarizing, the ingredients of the proposed approach are: a RANS closure model, a SGS model for LES and the definition of the blending function.

As far the closure of the RANS equations is concerned, in the present study, the standard $k-\varepsilon$ model Ref. [15] is used, in which the Reynolds stress tensor is modeled by introducing a turbulent eddy-viscosity μ_t, defined as a function of the turbulent kinetic energy k and of the turbulent dissipation rate of energy, ε, as follows:

$$\mu_t = C_\mu \frac{k^2}{\varepsilon} \tag{5}$$

where C_μ is a model parameter, set here equal to the classical value of 0.09 and k and ε are obtained from the corresponding modeled transport equations (see Ref. [15]).

For the LES mode, we wish to recover the Variational Multi-Scale approach Ref. [11], in which the flow variables are decomposed as follows:

$$w_i = \underbrace{\overline{w}_i}_{LRS} + \underbrace{w_i'}_{SRS} + {w_i}^{SGS} \tag{6}$$

where $\overline{w}_i$ are the large resolved scales (LRS), w_i' are the small resolved scales (SRS). This decomposition is obtained by variational projection in the LRS and SRS spaces respectively. In the present study, we follow the VMS approach proposed in Ref. [12] for the simulation of compressible turbulent flows through a finite volume/finite element discretization on unstructured tetrahedral grids.

If χ_l are the N finite-volume basis functions and ϕ_l the N finite-element basis functions associated to the used grid, the Galerkin approximation of the Navier-Stokes equations can be written as follows:

$$\left(\frac{\partial \boldsymbol{W}}{\partial t}, \chi_l\right) \; + \; (\nabla \cdot F_c(\boldsymbol{W}), \chi_l) + (\nabla \cdot F_v(\boldsymbol{W}), \phi_l) \; = 0 \quad l = 1, N \tag{7}$$

where $(\cdot, \cdot)$ denotes the L^2 scalar product, $F_c(\boldsymbol{W})$ are the convective fluxes, discretized by finite volumes and $F_v(\boldsymbol{W})$ are the viscous fluxes, discretized by finite elements. In order to obtain the VMS flow decomposition in Eq. (6), the finite dimensional spaces $\mathcal{V}_{FV}$ and $\mathcal{V}_{FE}$, respectively spanned by χ_l and ϕ_l, can be in turn decomposed as follows Ref. [12]:

$$\mathcal{V}_{FV} = \overline{\mathcal{V}}_{FV} \bigoplus \mathcal{V}'_{FV} \; ; \quad \mathcal{V}_{FE} = \overline{\mathcal{V}}_{FE} \bigoplus \mathcal{V}'_{FE} \tag{8}$$

in which $\bigoplus$ denotes the direct sum and $\overline{\mathcal{V}}_{FV}$ and $\mathcal{V}'_{FV}$ are the finite volume spaces associated to the largest and smallest resolved scales, spanned by the basis functions $\overline{\chi_l}$ and χ'_l; $\overline{\mathcal{V}}_{FE}$ and $\mathcal{V}'_{FE}$ are the finite element analogous. In Ref. [12] a projector operator P in the LRS space is defined by spatial average on macro cells in the following way:

$$\overline{\boldsymbol{W}} = P(\boldsymbol{W}) = \sum_k \underbrace{\left(\frac{Vol(C_k)}{\sum_{j \epsilon I_k} Vol(C_j)} \sum_{j \epsilon I_k} \chi_j \right)}_{\overline{\chi}_k} \boldsymbol{W}_k \tag{9}$$

for the convective terms, discretized by finite volumes, and:

$$\overline{\boldsymbol{W}} = P(\boldsymbol{W}) = \sum_k \underbrace{\left(\frac{Vol(C_k)}{\sum_{j \epsilon I_k} Vol(C_j)} \sum_{j \epsilon I_k} \phi_j \right)}_{\overline{\phi}_k} \boldsymbol{W}_k \tag{10}$$

for the diffusive terms, discretized by finite volumes. In both Eqs. (9) and (10), C_j is the finite volume cell around the node j, $Vol(C_j)$ denotes its volume and $I_k = \{j / C_j \in C_{m(k)}\}$, $C_{m(k)}$ being the macro-cell containing the cell C_k. The macro-cells are obtained by a process known as agglomeration Ref. [14]. The basis functions for the SRS space are clearly obtained as follows: $\chi'_l = \chi_l - \overline{\chi}_l$ and $\phi'_l = \phi_l - \overline{\phi}_l$.

Finally, in the VMS approach the SGS model is added only to the smallest resolved scales. As in Ref. [12], the Smagorinsky model is used, and, hence, the SGS terms are discretized analogously to the viscous fluxes. Thus, the Galerkin projection of Eq. (2) becomes:

$$\begin{array}{l} \left(\dfrac{\partial \langle \boldsymbol{W} \rangle + \boldsymbol{W}^c}{\partial t}, \chi_l\right) + (\nabla \cdot F_c(\langle \boldsymbol{W} \rangle + \boldsymbol{W}^c), \chi_l) + \\ (\nabla \cdot F_v(\langle \boldsymbol{W} \rangle + \boldsymbol{W}^c), \phi_l) = - \left(\; \tau^{LES}(\boldsymbol{W}'), \phi'_l \right) \quad l = 1, N \end{array} \tag{11}$$

in which τ_{LES} is modeled by introducing a SGS eddy-viscosity μ_s. The Smagorinsky SGS model Ref. [21] is adopted here; thus, we have:

$$\mu_s = \rho' C_s \Delta^2 \sqrt{S'_{ij} S'_{ij}} \tag{12}$$

where C_s is the model input parameter, S'_{ij} is the strain-rate tensor (computed in the VMS approach as a function of $\boldsymbol{W}'$ and Δ is a length which should be representative of the size of the resolved turbulent scales. Here, Δ has been selected as $Vol(i)^{1/3}$ (that is the volume of the i-th tetrahedral element) and C_s has been set equal to 0.1.

Finally, the Galerkin projection of Eqs. (1) and (4) for the computation of $\langle \boldsymbol{W} \rangle$ and of the additional fluctuations in the proposed hybrid model become respectively:

$$\begin{array}{l} \left(\dfrac{\partial \langle \boldsymbol{W} \rangle}{\partial t}, \chi_l \right) + (\nabla \cdot F_c(\langle \boldsymbol{W} \rangle), \chi_l) + (\nabla \cdot F_v(\langle \boldsymbol{W} \rangle), \phi_l) = \\ - \left(\tau^{RANS}(\langle \boldsymbol{W} \rangle), \phi_l \right) \quad l = 1, N \end{array} \tag{13}$$

$$\begin{array}{l} \left(\dfrac{\partial \boldsymbol{W}^c}{\partial t}, \chi_l \right) + (\nabla \cdot F_c(\langle \boldsymbol{W} \rangle + \boldsymbol{W}^c), \chi_l) - (\nabla \cdot F_c(\langle \boldsymbol{W} \rangle), \chi_l) + \\ (\nabla \cdot F_v(\boldsymbol{W}^c), \phi_l) = (1 - \theta) \left[\left(\tau^{RANS}(\langle \boldsymbol{W} \rangle), \phi_l \right) - \left(\tau^{LES}(\boldsymbol{W}'), \phi'_l \right) \right] \quad l = 1, N \end{array} \tag{14}$$

2.1 Definition of the blending function

As a possible choice for θ, the following function is used in the present study:

$$\theta = F(\xi) = tanh(\xi^2) \tag{15}$$

where ξ is the *blending parameter*, which should indicate whether the grid resolution is fine enough to resolve a significant part of the turbulence fluctuations, i.e. to obtain a LES-like simulation. The choice of the *blending parameter* is clearly a key point for the definition of the present hybrid model. In the present study, different options are proposed and investigated, namely:

- $\xi = \dfrac{\mu_s}{\mu_t}$, which is also used as a blending parameter in LNS Ref. [1],
- $\xi = \dfrac{\Delta}{l_{RANS}}$, l_{RANS} being a typical length in the RANS approach, i.e. $l_{RANS} = \dfrac{k^{3/2}}{\epsilon}$
- $\xi = \dfrac{t_{LES}}{t_{RANS}}$, t_{LES} and t_{RANS} being characteristic times of the LES and RANS approaches respectively, $t_{LES} = \dfrac{1}{\sqrt{S'_{ij} S'_{ij}}}$ and $t_{RANS} = \dfrac{k}{\epsilon}$.

2.2 Simplified model

To avoid the solution of two different systems of PDE and the consequent increase of required computational resources, Eqs. (13) and (14) can be recast together as follows:

$$\begin{aligned}&\left(\frac{\partial \boldsymbol{W}}{\partial t}, \chi_l\right) + (\nabla \cdot F_c(\boldsymbol{W}), \chi_l) + (\nabla \cdot F_v(\boldsymbol{W}), \phi_l) = \\ &-\theta \left(\tau^{RANS}(\langle \boldsymbol{W} \rangle), \phi_l\right) - (1-\theta) \left(\tau^{LES}(\boldsymbol{W}'), \phi_l'\right) \quad l = 1, N\end{aligned} \tag{16}$$

Clearly, if only Eq. (16) is solved, $\langle \boldsymbol{W} \rangle$ is not available at each time step. Two different options are possible: either to use an approximation of $\langle \boldsymbol{W} \rangle$ obtained by averaging and smoothing of $\boldsymbol{W}$, in the spirit of VMS, or to simply use in Eq. (16) $\tau^{RANS}(\boldsymbol{W})$. The second option is adopted in the present study as a first approximation.

3 LNS approach

The Reynolds-Averaged Navier-Stokes equations for compressible flows of (calorically and thermally) perfect Newtonian gases are considered here, written in conservative form in the following variables: density (ρ), momentum (ρu_i, $i = 1, 2, 3$) and total energy per unit volume ($E = \rho e + 1/2 \rho u_i u_i$, e being the internal energy).

The standard $k-\varepsilon$ model Ref. [15] is used for the closure of the RANS equations, in which the Reynolds stress tensor is modeled as follows, by introducing a turbulent eddy-viscosity, μ_t:

$$R_{ij} \simeq \mu_{\mathrm{t}} \underbrace{\left[\frac{\partial \widetilde{u}_i}{\partial x_j} + \frac{\partial \widetilde{u}_j}{\partial x_i} - \frac{2}{3} \frac{\partial \widetilde{u}_l}{\partial x_l} \delta_{ij} \right]}_{\widetilde{P}_{ij}} - \frac{2}{3} \overline{\rho} k \delta_{ij} \quad , \tag{17}$$

in which the tilde denotes the Favre average, the overbar time averaging, δ_{ij} is the Krönecker symbol and k is the turbulent kinetic energy. The turbulent eddy-viscosity μ_{t} is defined as a function of k and of the turbulent dissipation rate of energy, ε, as in Eq. (5).

In the LNS model the Reynolds stress tensor given by the RANS closure is multiplied by a blending function. Thus, the LNS equations are obtained from the RANS ones by replacing the Reynolds stress tensor R_{ij}, given by Eq. (17), with the tensor L_{ij}:

$$L_{ij} = \alpha R_{ij} = \alpha \mu_t \widetilde{P}_{ij} - \frac{2}{3} \overline{\rho} \left(\alpha k \right) \delta_{ij} \quad , \tag{18}$$

where α is the damping function ($0 \leq \alpha \leq 1$), varying in space and time.

In the LNS model proposed in Ref. [1], the damping function is defined as follows:

$$\alpha = \min \left\{ \frac{\mu_s}{\mu_t}, 1 \right\} \tag{19}$$

in which μ_s is the SGS viscosity obtained from Eq.12 with the only difference that here Δ has been selected, for each tetrahedral element of the grid, as the length of the longest edge (see Ref. [4]).

The set of LNS equations is reported here for sake of completeness:

$$\frac{\partial \overline{\rho}}{\partial t} + \frac{\partial \overline{\rho}\widetilde{u}_i}{\partial x_i} = 0 \quad , \tag{20}$$

$$\frac{\partial \overline{\rho}\widetilde{u}_i}{\partial t} + \frac{\partial \rho \widetilde{u}_i \widetilde{u}_j}{\partial x_j} = -\frac{\partial \overline{p}}{\partial x_i} + \frac{\partial (\widetilde{\sigma}_{ij} + L_{ij})}{\partial x_j} \quad , \tag{21}$$

$$\begin{aligned} \frac{\partial \overline{E}}{\partial t} + \frac{\partial \widetilde{u}_j \left(\overline{E} + \overline{p}\right)}{\partial x_j} =& \frac{\partial \widetilde{u}_i \widetilde{\sigma}_{ij}}{\partial x_j} + \frac{\partial \widetilde{u}_i L_{ij}}{\partial x_j} + \frac{\partial}{\partial x_j}\left(\frac{\alpha \mu_{\mathrm{t}}}{\sigma_k}\frac{\partial k}{\partial x_j}\right) + \\ & \frac{\partial}{\partial x_j}\left(\frac{C_p}{Pr}\left(\mu + \alpha\mu_{\mathrm{t}}\right)\frac{\partial \widetilde{T}}{\partial x_j}\right) = 0 \end{aligned} \quad , \tag{22}$$

$$\frac{\partial \overline{\rho} k}{\partial t} + \frac{\partial \overline{\rho}\widetilde{u}_j k}{\partial x_j} = \frac{\partial}{\partial x_j}\left[\left(\mu + \frac{\alpha\mu_{\mathrm{t}}}{\sigma_k}\right)\frac{\partial k}{\partial x_j}\right] + L_{ij}\frac{\partial \widetilde{u}_i}{\partial x_j} - \overline{\rho}\varepsilon \quad , \tag{23}$$

$$\frac{\partial \overline{\rho} \varepsilon}{\partial t} + \frac{\partial \overline{\rho}\varepsilon\widetilde{u}_j}{\partial x_j} = \frac{\partial}{\partial x_j}\left[\left(\mu + \frac{\alpha\mu_{\mathrm{t}}}{\sigma_\epsilon}\right)\frac{\partial \varepsilon}{\partial x_j}\right] + C_{\epsilon 1}\left(\frac{\varepsilon}{k}\right)L_{ij}\frac{\partial \widetilde{u}_i}{\partial x_j} - C_{\epsilon 2}\overline{\rho}\frac{\varepsilon^2}{k} \quad . \tag{24}$$

in which p is the pressure, σ_{ij} the viscous-stress tensor, μ the molecular viscosity, C_p the specific heat at constant pressure, T the temperature and Pr_t the turbulent Prandtl number. The following values have been used for the different parameters in the k and ε equations: $\sigma_\epsilon = 1.4245$, $C_{\epsilon 1} = 1.44$ and $C_{\epsilon 2} = 11/6$.

Summarizing, wherever the LES SGS-viscosity is lower than the RANS eddy-viscosity ($\alpha < 1$), an expression very similar to the classical Smagorinsky model is obtained for the turbulent stresses by combining Eqs. (17), (18) and(19). The difference with the classical Smagorinsky model is the presence of the diagonal term proportional to k. However, for compressible flows, this can be considered as a model for the isotropic part of the SGS stresses. As discussed in Ref. [1], the model should work in the LES mode where the grid is fine enough to resolve a significant part of the turbulence scales, as in LES; elsewhere ($\alpha = 1$), the $k - \varepsilon$ RANS closure is recovered.

Note that in LNS R_{ij} is replaced with L_{ij} not only in the momentum and energy equations, but also in the two additional equations in k and ε. This implies that, although the total turbulent kinetic energy dissipates at the rate dictated by ε, the energy-production term $R_{ij}\frac{\partial \widetilde{u}_i}{\partial j}$ is replaced by $L_{ij}\frac{\partial \widetilde{u}_i}{\partial j} = \alpha R_{ij}\frac{\partial \widetilde{u}_i}{\partial j}$. Consequently, a reduction of the turbulent kinetic energy production is obtained in those regions where a fraction of turbulence is directly simulated ($\alpha < 1$).

A reduction of the turbulent transport of k and ε in regions where $\alpha < 1$ is also obtained by replacing μ_{t} with $\alpha\mu_{\mathrm{t}}$ in the RANS equations for k and ε.

Finally, one can notice that, by construction, the present version of the LNS model is no more time consuming than the RANS $k - \epsilon$ model. Indeed, the extra-cost due to the evaluation of the Smagorinsky eddy viscosity is negligible compared to the overall computation required by the solution of the RANS $k - \epsilon$ equations.

4 Numerical method

The governing equations have been discretized in space using a mixed finite-volume/finite-element method applied to unstructured tetrahedrizations. The adopted scheme is vertex centered, i.e. all degrees of freedom are located at the vertices. P1 Galerkin finite elements are used to discretize the diffusive terms.

A dual finite-volume grid is obtained by building a cell C_i around each vertex i through the rule of medians. The convective fluxes are discretized on this tessellation, i.e. in terms of fluxes relative to the common boundaries shared by neighboring cells.

The Roe scheme Ref. [20] represents the basic upwind component for the numerical evaluation of the convective fluxes $\mathcal{F}$:

$$\Phi^R\left(W_i,\ W_j,\ \vec{n}\right) = \frac{\mathcal{F}\left(W_i,\ \vec{n}\right) + \mathcal{F}\left(W_j,\ \vec{n}\right)}{2} - \gamma_s \left[P^{-1}|P\mathcal{R}|\ \frac{W_j - W_i}{2} \right] \tag{25}$$

in which $\Phi^R\left(W_i,\ W_j,\ \vec{n}\right)$ is the numerical approximation of the flux between the i-th and the j-th cells, W_i is the solution vector at the i-th node, $\vec{n}$ is the outward normal to the cell boundary and $\mathcal{R}\left(W_i,\ W_j,\ \vec{n}\right)$ is the Roe Matrix. The matrix $P(W_i,\ W_j)$ is the Turkel-type preconditioning term, introduced to avoid accuracy problems at low Mach numbers Ref. [9]. Note that, since it only appears in the upwind part of the numerical fluxes, the scheme remains consistent in time and can thus be used for unsteady flow simulations. Finally, the parameter γ_s, which multiplies the upwind part of the scheme, collected within square brackets in Eq. (25), permits a direct control of the numerical viscosity, leading to a full upwind scheme for $\gamma_s = 1$ and to a centered scheme when $\gamma_s = 0$. The spatial accuracy of this scheme is only first order. The MUSCL linear reconstruction method ("Monotone Upwind Schemes for Conservation Laws"), introduced by Van Leer Ref. [24], is therefore employed to increase the order of accuracy of the Roe scheme. This is obtained by expressing the Roe flux between two cells, centered on two generic nodes i and j, as a function of the reconstructed values of W at their interface: $\Phi^R\left(W_{ij},\ W_{ji},\ \vec{n}_{ij}\right)$, where W_{ij} is extrapolated from the values of W at nodes i and j. A reconstruction using a combination of different families of approximate gradients (P1-elementwise gradients and nodal gradients evaluated on different tetrahedra) is adopted, which allows a numerical dissipation made of sixth-order space derivatives to be obtained. The MUSCL reconstruction is described in detail in Ref. [6], in which the capabilities of this scheme in concentrating the numerical viscosity effect on a narrow-band of the highest resolved frequencies is also discussed. As discussed in Ref. [6], this is specially important in LES simulations to limit as far as possible the interactions between numerical and SGS dissipation, which could deteriorate the accuracy of the results.

Either implicit or explicit schemes can be used to advance the equations in time by a line method, i.e. time and space are treated separately. In the explicit case a N-stage low-storage Runge-Kutta algorithm is available, in which the number of stages and the coefficients can be varied to obtain different schemes. An implicit time marching algorithm is also available in the code, based on a second-order time-accurate backward difference

scheme. A first-order semi-discretization of the jacobians is used together with a defect-correction procedure Ref. [17]; the resulting scheme is linearly unconditionally stable and second-order accurate.

More details on the numerical ingredients used in the present work can be found in Ref. [4, 8].

	l_i/D	l_o/D	H_y/D	H_z/D	N. nodes	N. elements
Gr1	4.5	9.5	7	9.75	8.3×10^4	4.75×10^5
Gr2	4.5	9.5	7	9.75	3.5×10^4	1.9×10^5

Table 1: Main feature of the computational domains and grids

5 Test-case description and simulation parameters

The flow around a square cylinder of infinite length is considered. The Reynolds number, based on the cylinder side length and on the free-stream velocity, is equal to 22000 and the used computational domain is represented in Fig. 1, together with the frame of reference.

With reference to Fig. 1, the domain dimensions are the following: $L_i/D = 4.5$, $L_o/D = 9.5$, $H_y/D = 7$, $H_z/D = 9.75$ (where z is for the span-wise direction). They are equal to those employed in the LNS simulation in Ref. [7].

The computational domain in Fig. 1 is discretized by generating two unstructured grids made of tetrahedral elements (grid GR1 and GR2 in Tab. 1). The two grids have a different resolution in order to test the influence of this parameter on the model. The section $z = 0$ of the first grid and $z = 4.875$ of the second are reported in Fig. 2(a),(b).

Approximate boundary conditions, based on the Reichardt wall-law Ref. [10], [18], are applied at the solid walls. The boundary treatment is controlled by the parameter δ, which sets the distance from the wall at which slip conditions are imposed. The velocity is assumed to vanish at the wall, starting by the value computed at the distance δ, by following the Reichardt wall-law. Appropriate values of the shear stress are obtained and used in the simulations as boundary condition. This law has the advantage of describing the velocity profile not only in the logarithmic region of a boundary layer but also in the laminar sublayer and in the intermediate region. This type of wall treatment has been successfully used in previous LES (Ref. [5], [6], [12]), RANS ([18], [19]) and LNS (Ref. [7]) simulations of the same flow. Finally, this approach allows the same boundary conditions to be used for both the RANS closure and the LES Smagorinsky model. At the inflow, the flow is assumed to be undisturbed and the Steger-Warming Ref. [23] conditions are applied. Boundary conditions based on the Steger-Warming decomposition are used at the outflow as well. On the other surfaces ($y = \pm H_y$, $z = \pm H_z$) slip conditions are imposed.

For both grids, the computations have been carried out using the LNS model and the new proposed hybrid model with the three different definitions of the blending parameter.

The simulations have been initialized with different values of k_0 (the initialization of the kinetic energy for the $k - \varepsilon$ RANS model) and δ (the parameter of the wall-law) to test the sensitivity of the model to these features.

Following the LNS work in Ref. [7], the numerical parameter γ, which controls the amount of numerical viscosity introduced in the simulation, has been set equal to 0.1 for GR1 and 0.5 for GR2, in order to obtain stable simulations.

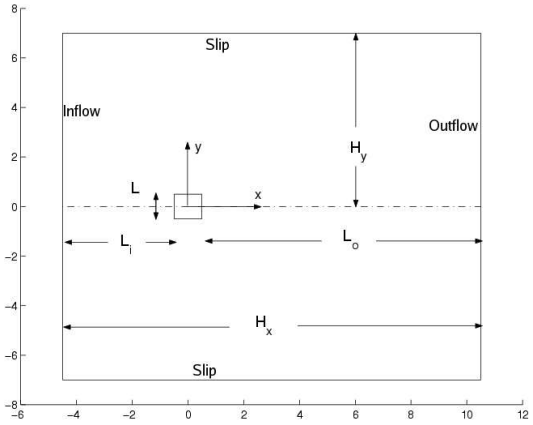

Figure 1: Computational domain (side view)

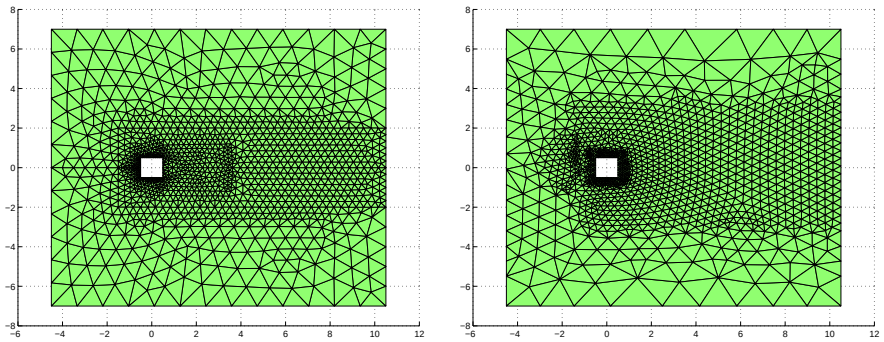

(a) (b)

Figure 2: grid GR1(a) and GR2 (b)

Simulations	Grid	δ	γ	CFL	Model	k_0
LNS2	Gr1	0.0041	0.1	10	LNS	$U_0/1000$
LNS3	Gr1	0.02	0.1	10	LNS	$U_0/1000$
LNS5	Gr2	0.02	0.5	10	LNS	$U_0/1000$
LNS6	Gr2	0.02	0.5	10	LNS	$U_0/10000$
BLE1	Gr1	0.0041	0.1	10	$\tanh((\nu_{VMS-LES}/\nu_{k-\varepsilon})^2)$	$U_0/1000$
BLE2	Gr1	0.02	0.1	10	$\tanh((\nu_{VMS-LES}/\nu_{k-\varepsilon})^2)$	$U_0/1000$
BLE4	Gr1	0.0041	0.1	20	$\tanh((t_{VMS-LES}/t_{k-\varepsilon})^2)$	$U_0/1000$
BLE5	Gr1	0.02	0.1	10	$\tanh((t_{VMS-LES}/t_{k-\varepsilon})^2)$	$U_0/1000$
BLE6	Gr2	0.06	0.5	10	$\tanh((\nu_{VMS-LES}/\nu_{k-\varepsilon})^2)$	$U_0/1000$
BLE7	Gr2	0.02	0.5	10	$\tanh((\nu_{VMS-LES}/\nu_{k-\varepsilon})^2)$	$U_0/1000$
BLE8	Gr2	0.02	0.5	10	$\tanh((\nu_{VMS-LES}/\nu_{k-\varepsilon})^2)$	$U_0/10000$
BLE9	Gr2	0.02	0.5	10	$\tanh((t_{VMS-LES}/t_{k-\varepsilon})^2)$	$U_0/1000$
BLE10	Gr2	0.02	0.5	10	$\tanh((t_{VMS-LES}/t_{k-\varepsilon})^2)$	$U_0/10000$
BLE11	Gr2	0.02	0.5	10	$\tanh((L_{VMS-LES}/L_{k-\varepsilon})^2)$	$U_0/1000$
BLE12	Gr2	0.02	0.5	10	$\tanh((L_{VMS-LES}/L_{k-\varepsilon})^2)$	$U_0/10000$

Table 2: Simulation parameters

The simulations have been implicitly advanced in time, with a maximum CFL number in the range from 10 to 20. In a previous work (Ref. [7]), it was shown that no significant information is lost in time provided that CFL$\leq$ 25.

The parameters characterizing the different simulations are summarized in Tab. 2.

Simulations	$\overline{C_d}$	C'_d	C'_l	St	l_r
LNS2	2.02	0.158	1.032	0.127	1.60
LNS3	2.11	0.116	0.654	0.131	1.15
LNS5	2.07	0.087	0.685	0.130	1.19
LNS6	2.08	0.086	0.628	0.136	1.01
BLE1	1.90	0.145	0.897	0.128	1.65
BLE2	1.95	0.107	0.810	0.130	1.37
BLE4	1.86	0.156	1.023	0.126	1.69
BLE5	2.01	0.117	0.792	0.131	1.16
BLE6	1.97	0.063	0.545	0.127	1.24
BLE7	2.01	0.074	0.580	0.129	1.13
BLE8	2.01	0.072	0.600	0.129	1.10
BLE9	2.01	0.071	0.600	0.131	1.21
BLE10	2.01	0.073	0.600	0.129	1.16
BLE11	2.01	0.083	0.630	0.128	1.05
BLE12	2.02	0.077	0.620	0.129	1.10
Exp.(Bearman and Obasaju 1982)	2.28		1.2	0.130	
Exp.(Lyn and Rody 1994)	2.1			0.132	1.4

Table 3: Simulation results

6 Results

A brief summary of the global parameters obtained in the different simulations and of some experimental data can be found in Tab.3. In particular, the sensitivity to the hybridization model, to δ and to k_0 are investigated. For each of the considered cases, figures showing the iso-contours of the blending parameter and of the LES or RANS eddy viscosities are reported, in order to highligth the behavior of the different considered hybridization strategies. Some mean velocity profiles are also shown and compared to experimental data.

6.1 Model influence

The model influence was tested for both grids. For the grid GR1, it is possible to compare simulations BLE1 and BLE4, in which the blending parameter is based on the viscosity ratio (VR) and time ratio (TR) respectively, with the simulation LNS2, which employs the LNS model. Figure 3 and 4 show the blending parameter (a), the VMS-LES (c) and RANS (d) viscosity fields, for BLE1 and BLE4; in fig. 5 the viscosity fields (LES (a), RANS (b)) are plotted and also the isoline at LNS parameter $\alpha = 0.95$. This is a numerical threshold between the zones in which the LNS model works in LES or RANS mode. It's important to underline that LNS works only in RANS or in LES mode so is possible to define a value of threshold like that explained before. In the new proposed hybrid model this is not possible because the model works also in an hybrid mode as seen in Sec.2. The simulation BLE1 seems to work in LES mode in the whole domain except near the wall of the cylinder in which the RANS model is adopted (fig.3(b)) and in some part outside of the wake (upwind from the cylinder, in the shear layers and near the lateral boundary) where the hybrid mode is set. This is in accordance with the viscosity fields, μ_s being lower than μ_t in the wake and comparable in those points of the field where the model works in the hybrid mode. Looking at BLE4 the differences with respect to BLE1 are evident. In the wake the model works not only in LES mode but there are also hybrid and RANS zones, the zone using RANS in the shear layers is larger that previously and around the wall the RANS mode is only near the upwind corners. This configuration is not completely in accord with the viscosity fields because, for example, in the wake the VMS-LES viscosity is everywhere lower than the RANS one while the model works somewhere in RANS mode. Comparing the two simulations with the LNS it is possible to see that the behaviour of the LNS model in the wake and outside is similar to that of BLE1 but the zone around the cylinder is closer to that of BLE4. Looking at the numerical results, from Tab.3, it appears that in the LNS2 simulation a better prediction of the mean drag coefficient $\overline{C_d}$ is obtained than in BLE1 and BLE4. The rms values of lift and drag coefficient and of the Strouhal number obtained in the different simulations are very similar. The length of the recirculation bubble (l_r) is overestimated in all cases. Figure 6 shows the stream-wise velocity profiles along the center line (Fig. 6 (a)) and in the lateral direction at two different locations in the wake (x/h=1.25 in Fig. 6 (b) and x/h=2.5 in Fig. 6 (c)). It can be seen that the differences between the models are small. The overall agreement with the experiments may be considered satisfactory, except for the much higher recovery velocity obtained in all simulations with respect to the experiments. This

is, however, a discrepancy observed in almost all the previous simulations in the literature and is discussed, for instance, in Ref. [5].

Simulations BLE2 and BLE5 , using the same models as BLE1 and BLE4, but with a different δ, can be compared with LNS3.

Figure 7, 8 and 9 report the same quantities previously discussed for BLE1, BLE4, LNS2 and namely the blending parameter, the LES and RANS eddy-viscosity. It seems that the behaviour of the blending parameter is the same as that observed for the previous set of simulations except for the zone around the cylinder in BLE2 (7(b)), in which the model now works in the hybrid mode with only small RANS regions near the corner of the cylinder (fig.7 (b)).

The results, with reference to Tab.3, show that $\overline{C_d}$ is better predicted than previously in all the presently considered cases. As previously, the values of r.m.s. of the force coefficients and of the Strouhal number are very similar for the different simulations. The mean recirculation length obtained in BLE5 and LNS3 is the same and is lower than the experimental value. Conversely, the length obtained in BLE2 is very close to the experimental one. For the mean velocity profiles (shown in Fig. 10), the same considerations as previously can be made, except that in this case BLE2, i.e. the simulations employing the viscosity ratio as blending parameter, seems to give a better agreement with the experiments than the other models. It should also be underlined that the differences between LNS3 and BLE5 are very small. For the grid GR2, the simulations BLE7, BLE9 and BLE11, using VR, TR, and the length ratio (LR) respectively as blending parameters, can be compared with the LNS simulation LNS5 or BLE8, BLE10 and BLE12, which employ the same models as BLE7, BLE9 and BLE11 respectively, but with a different k_0, can be compared with LNS6. The global parameters (Tab.3) are very similar for all the different versions of the new hybrid model, but it seems that LR gives a slightly better prediction of the r.m.s. values of the force coefficients and TR of the mean recirculation length. However, the r.m.s. values of the force coefficients are underestimated in all the simulations and the best agreement with the experiments is obtained with LNS. The mean drag coefficient is well predicted in all the simulations, the maximum error is less than 4%. As it is possible to see in fig. 11 (a) (BLE7), fig. 12 (b) (BLE9) and fig. 13 (c) (BLE11), the hybrid based on TR and VR as blending parameters has a behaviour very similar to that one in grid GR1. In the other case (LR as blending parameter), into the wake the model works in VMS-LES mode. Starting from the upwind corner the wake is bounded by a RANS zone and then (most of all in the upwind part) there is a zone where the model works in an hybrid way. In the other part of the domain RANS mode is used. The velocity profiles, shown in Figs. 15 and 20, are also for this case not very sensitive to the model and the overall agreement with the experiments is rather satisfactory (except for the recovery velocity in the far wake, as previously discussed), especially for the very coarse considered grid.

6.2 Sensitivity to the inflow value of the turbulent kinetic energy, k_0

The sensitivity to the inflow value of the turbulent kinetic energy, k_0, was tested only on grid GR2. The numerical predictions of the flow global parameters (compare BLE7 vs BLE8 or BLE9 vs BLE10 or BLE11 vs BLE12 in Tab.2) seem not to be very sensitive to this parameter. Also, the mean velocity profiles obtained with different values of k_0 are very similar, as can be noticed by comparing fig.15 with fig.20. The only visible change is in the blending function behaviour: it seems that decreasing the value of k_0 there is a larger region outside the wake in which the RANS model is used (compare for example fig.13(a) with fig.18(a)). This is due to the different value of the RANS viscosity in the inlet part of the domain, compare for example fig.13(d) with fig.18(d). Indeed, it is possible to see that the RANS viscosity in BLE11 shows a step decrease in the inlet part that is not present in BLE12. This seems to indicate that in BLE11 the inlet value of k_0 is too high. However, the fact that the results are not sensitive to k_0 indicates that the proposed hybridization strategies does not require a fine tuning of the inlet RANS parameters, which is conversely important in pure RANS calculations.

6.3 Sensitivity to the parameter δ in the approximate wall treatment

The sensitivity to the parameter δ in the approximate wall treatment (see Sec. 5) was tested only on grid GR1. As for the global parameters (compare BLE1 with BLE2 or BLE4 with BLE5 in Tab.2), when δ is increased, the accuracy of the numerical prediction of $\overline{C_d}$, St and l_r seems to be improved, while that of the numerical prediction of the r.m.s. of the force coefficients seems to deteriorate. The blending parameter, as function of δ, changes its behaviour only in the zone near the cylinder: increasing δ the RANS zone decrease (compare fig. 3(a) with fig.7(a)). The mean velocity profiles are very sensitive to this parameter. The first comparison that can be made is between fig. 6(a) and fig. 10(a), which shows the x-component of the velocity (u) in the plane $y/L = 0$. Increasing δ the curves are translated backward with respect to the x axis and the slope is increased. Then, it is possible to compare fig. 6(b) and fig. 10(b), showing the u profile in the plane $x/L = 1.5$. Increasing δ there is a translation towards higher values near the middle of the wake ($y/L = 0$) and towards lower values outside (higher y). TR (BLE4 and BLE5) and LNS (LNS2 and LNS3), are subjected to larger variations than VR (BLE1 and BLE2). In addiction the behaviour of the profile of BLE1 and BLE2 seems closer to that of the experimental data. Looking at fig.6(c) and fig.10(c), in which the u profile of the plane $x/L = 2.5$ is reported, it can be seen that the results are also affected by δ. For example in the zone between $1 < y/L < 2.5$ the curves of the simulations with $\delta = 0.02$ are closer to the experimental data than those with $\delta = 0.0041$.

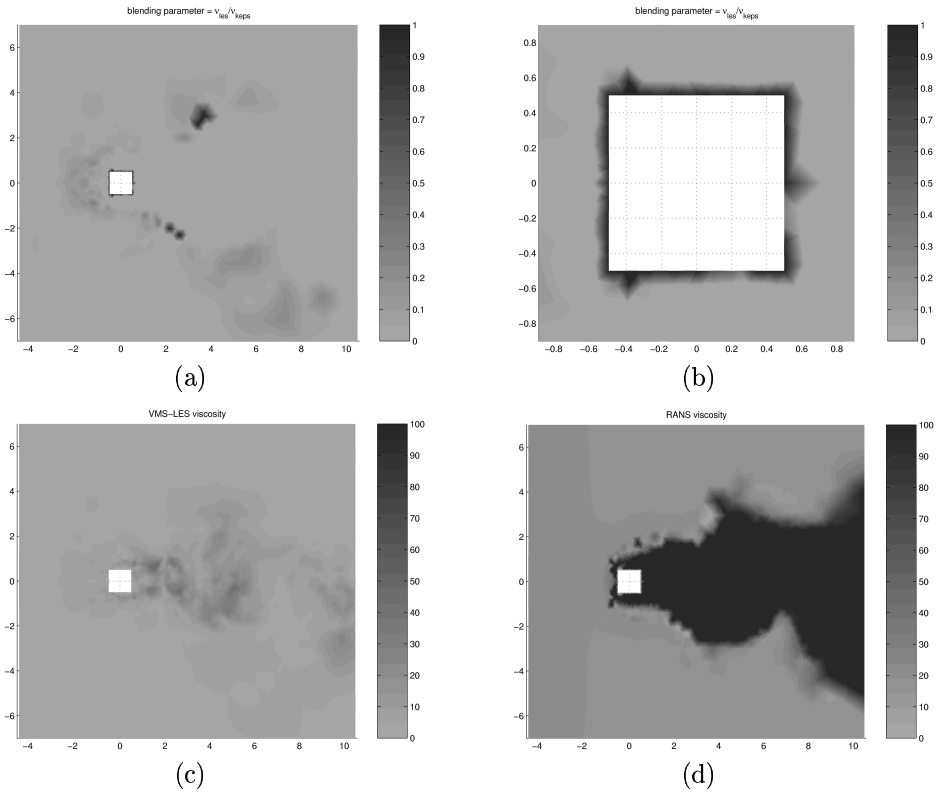

Figure 3: Plot of the blending parameter (a) and zoom around the cylinder (b), plot of the VMS-LES viscosity (c) and RANS viscosity for the BLE1 parameter.

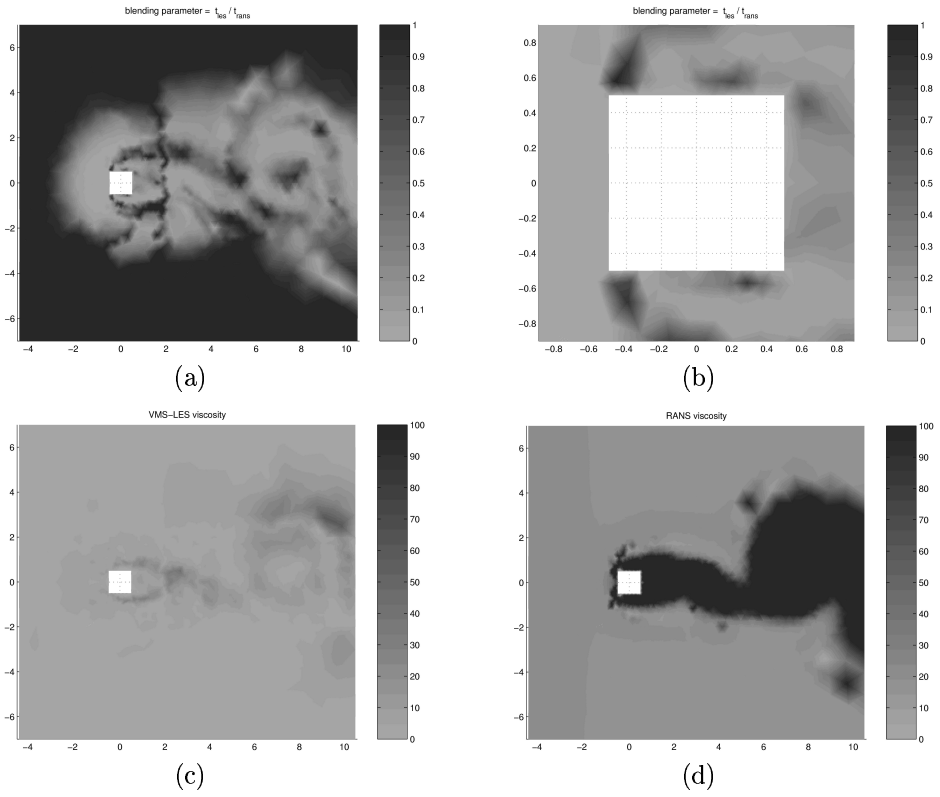

Figure 4: Plot of the blending parameter (a) and zoom around the cylinder (b), plot of the VMS-LES viscosity (c) and RANS viscosity for the BLE4 parameter.

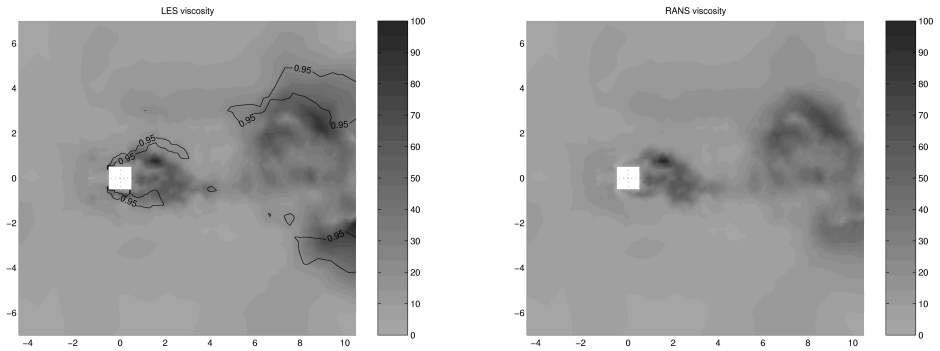

Figure 5: Plot of the VMS-LES viscosity with isoline at LNS parameter=0.95 (b) and RANS viscosity for the LNS2.

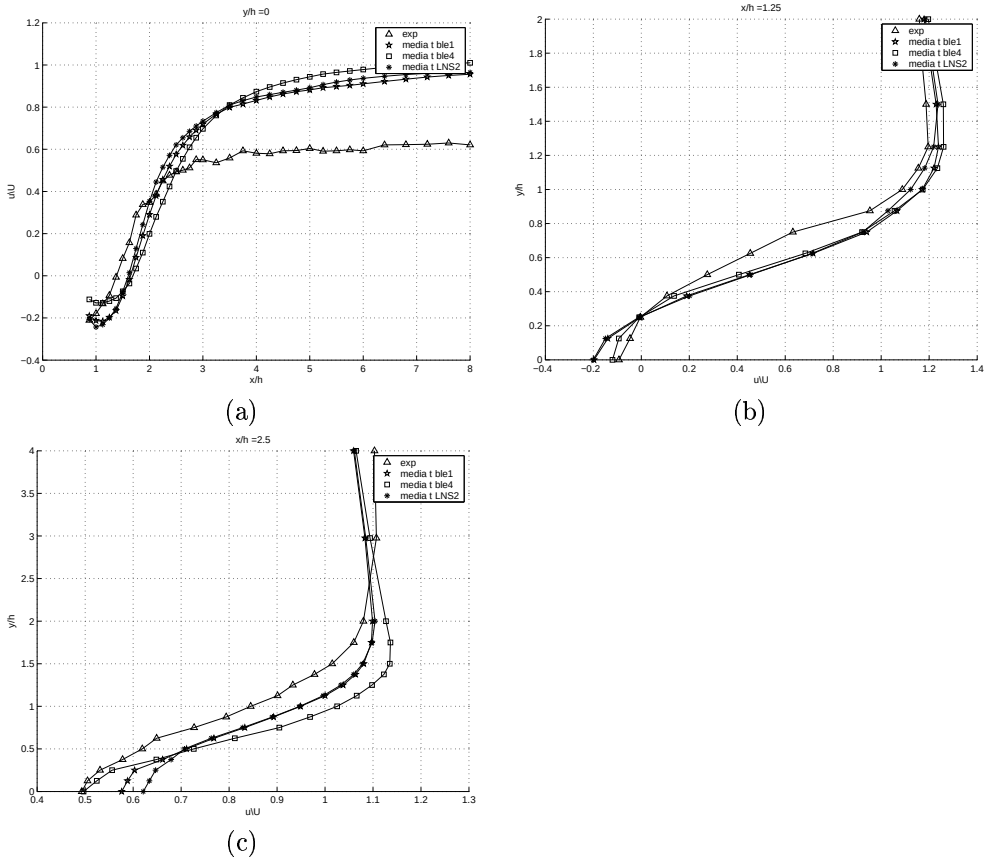

Figure 6: u velocity profiles for BLE1, BLE4 and LNS2 plane y/L=0 (a), x/L=1.25 (b), x/L=2.5 (c)

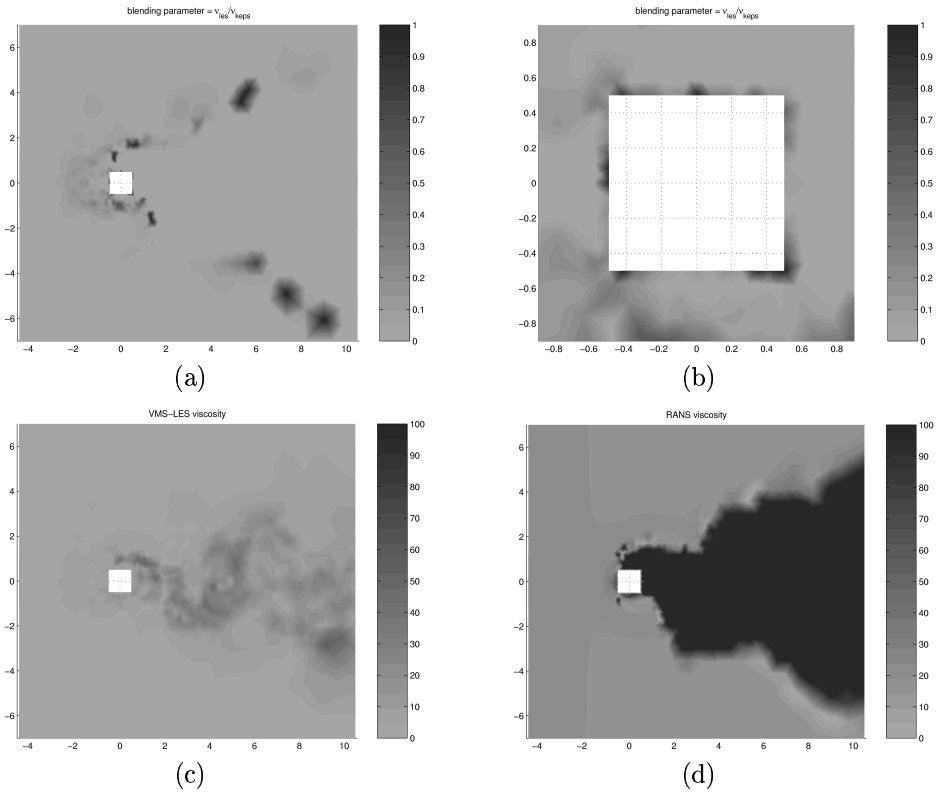

Figure 7: Plot of the blending parameter (a) and zoom around the cylinder (b), plot of the VMS-LES viscosity (c) and RANS viscosity for the BLE2 parameter.

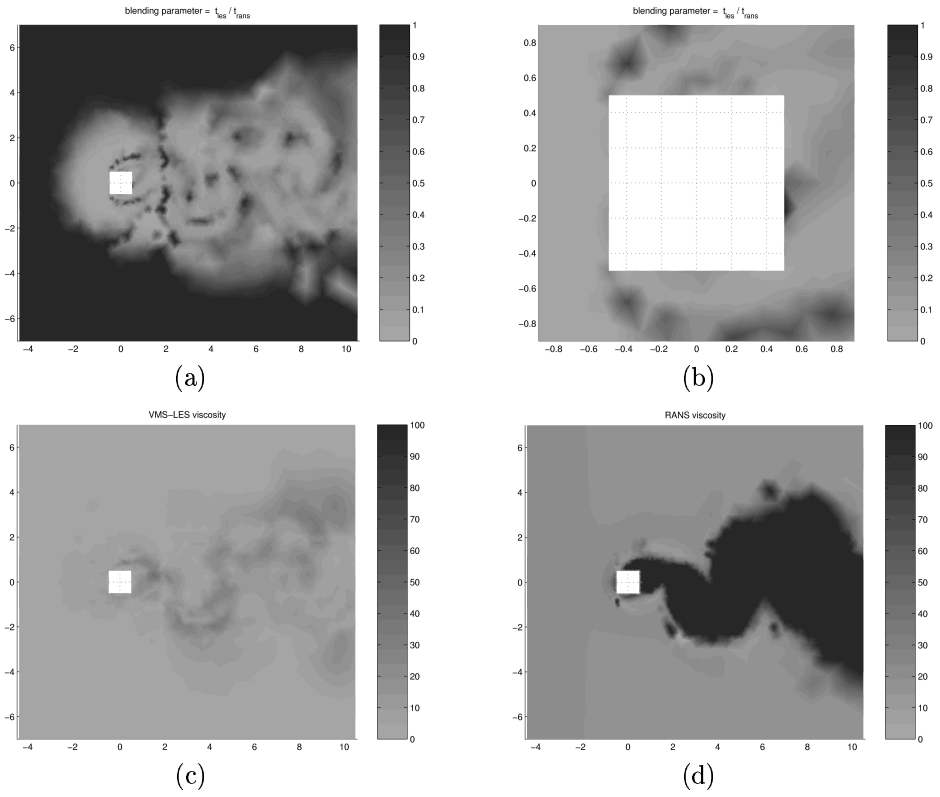

Figure 8: Plot of the blending parameter (a) and zoom around the cylinder (b), plot of the VMS-LES viscosity (c) and RANS viscosity for the BLE5 parameter.

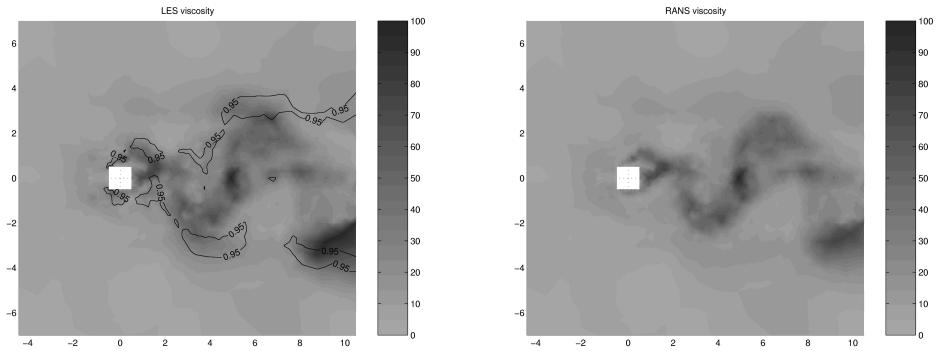

Figure 9: Plot of the VMS-LES viscosity with isoline at LNS parameter=0.95 (b) and RANS viscosity for the LNS3.

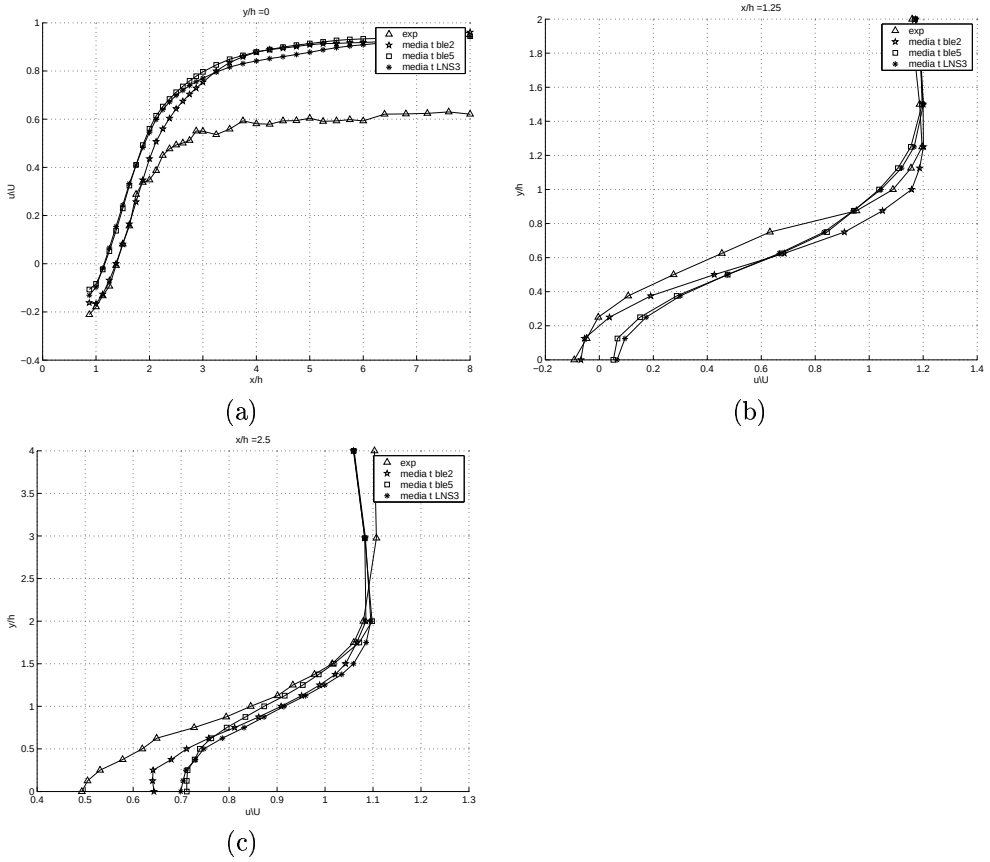

Figure 10: u velocity profiles for BLE2, BLE5 and LNS3 plane y/L=0 (a), x/L=1.25 (b), x/L=2.5 (c)

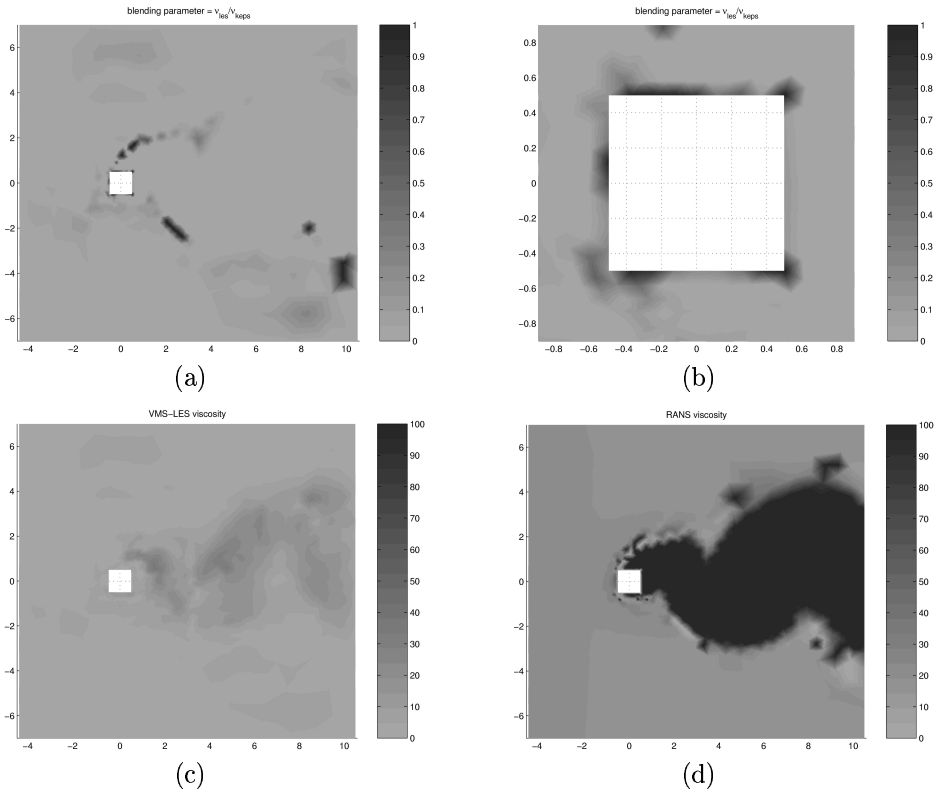

Figure 11: Plot of the blending parameter (a) and zoom around the cylinder (b), plot of the VMS-LES viscosity (c) and RANS viscosity for the BLE7 parameter.

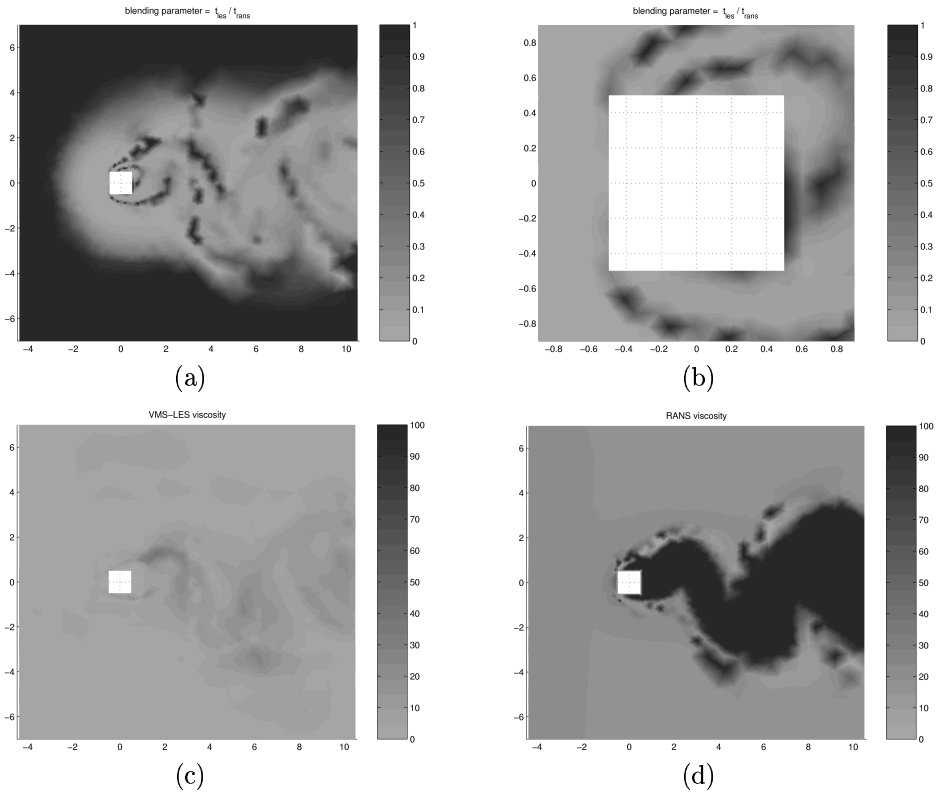

Figure 12: Plot of the blending parameter (a) and zoom around the cylinder (b), plot of the VMS-LES viscosity (c) and RANS viscosity for the BLE9 parameter.

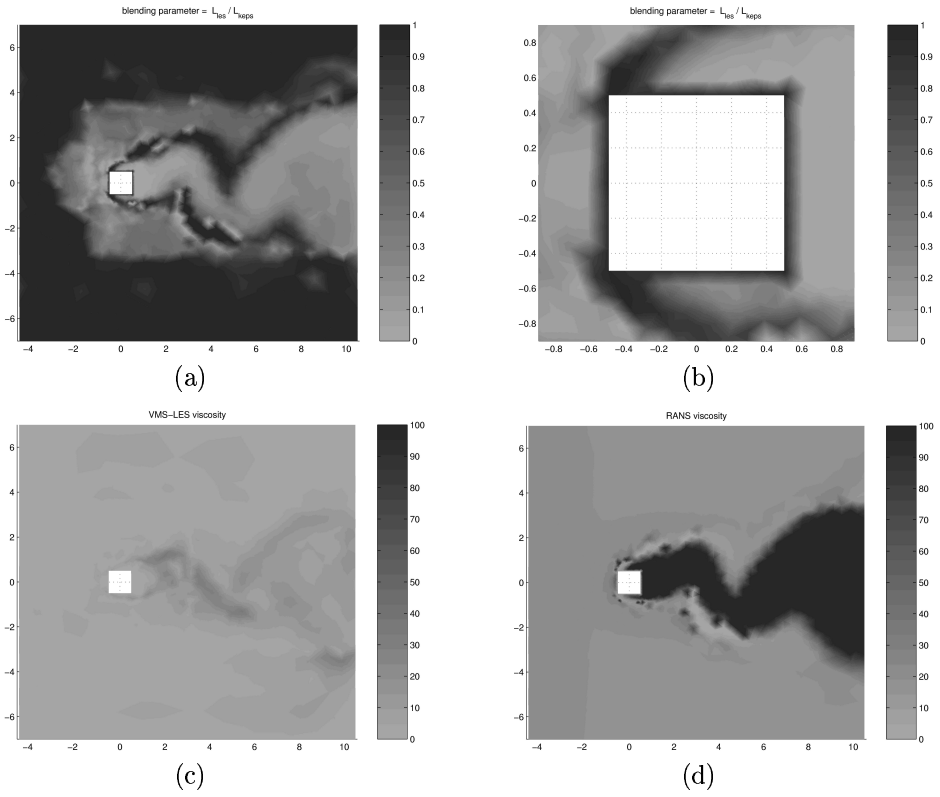

Figure 13: Plot of the blending parameter (a) and zoom around the cylinder (b), plot of the VMS-LES viscosity (c) and RANS viscosity for the BLE11 parameter.

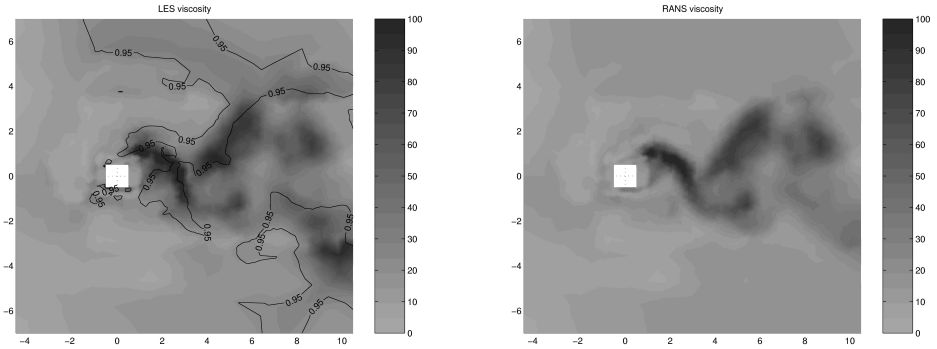

Figure 14: Plot of the VMS-LES viscosity with isoline at LNS parameter=0.95 (b) and RANS viscosity for the LNS5.

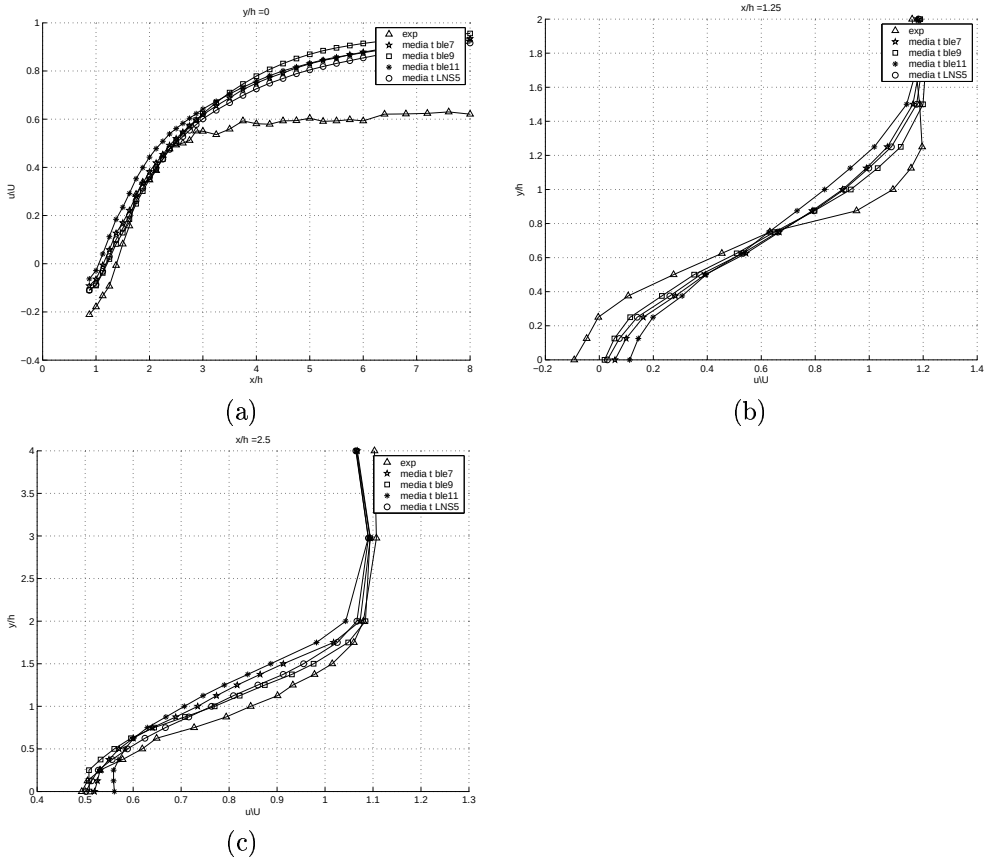

Figure 15: u velocity profiles for BLE7, BLE9, BLE11 and LNS5 plane y/L=0 (a), x/L=1.25 (b), x/L=2.5 (c)

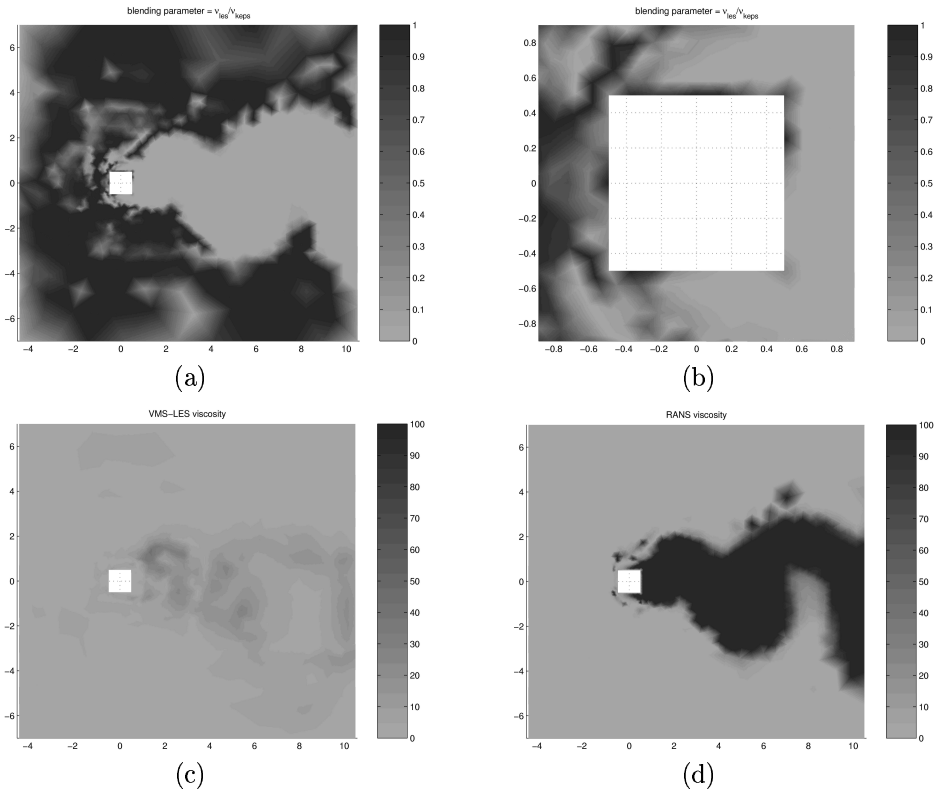

Figure 16: Plot of the blending parameter (a) and zoom around the cylinder (b), plot of the VMS-LES viscosity (c) and RANS viscosity for the BLE8 parameter.

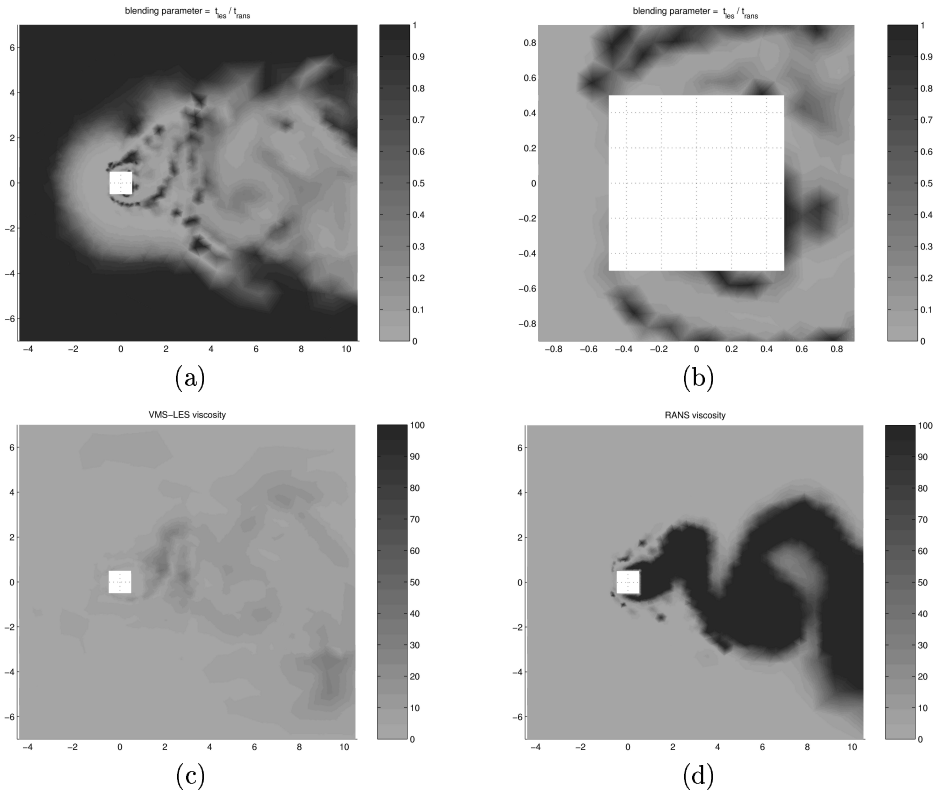

Figure 17: Plot of the blending parameter (a) and zoom around the cylinder (b), plot of the VMS-LES viscosity (c) and RANS viscosity for the BLE10 parameter.

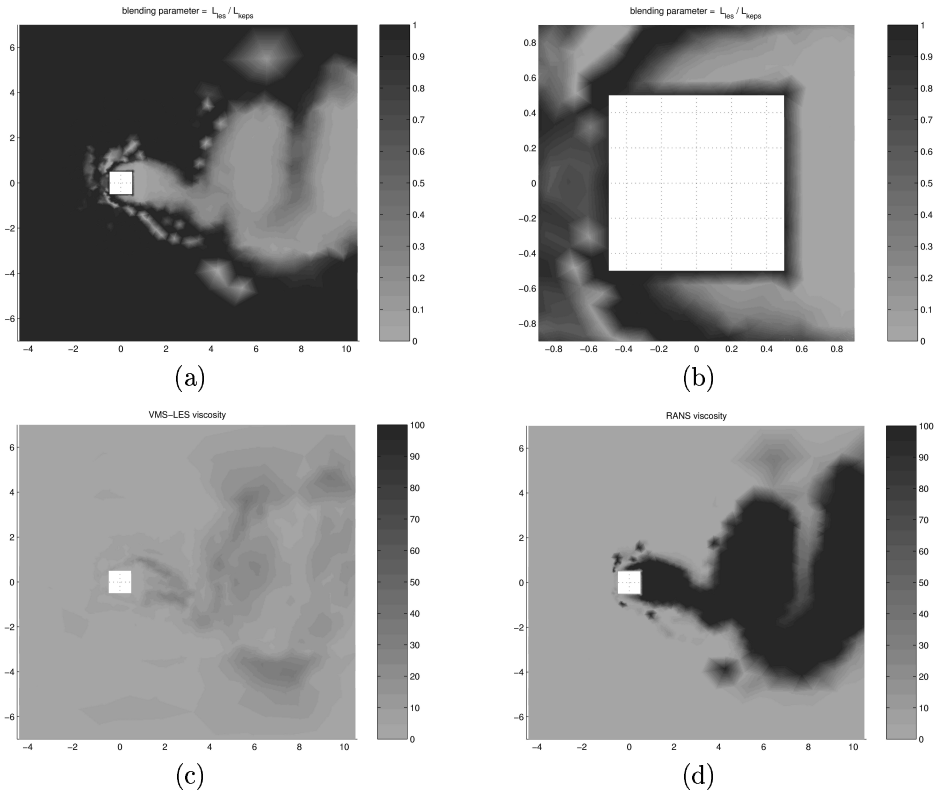

Figure 18: Plot of the blending parameter (a) and zoom around the cylinder (b), plot of the VMS-LES viscosity (c) and RANS viscosity for the BLE12 parameter.

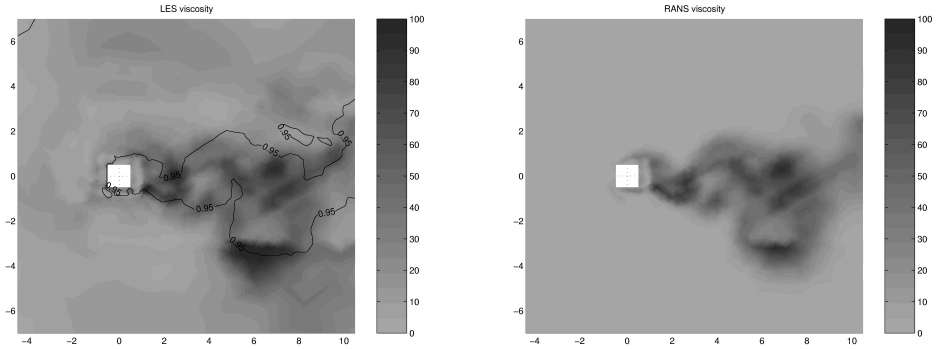

Figure 19: Plot of the VMS-LES viscosity with isoline at LNS parameter=0.95 (b) and RANS viscosity for the LNS6.

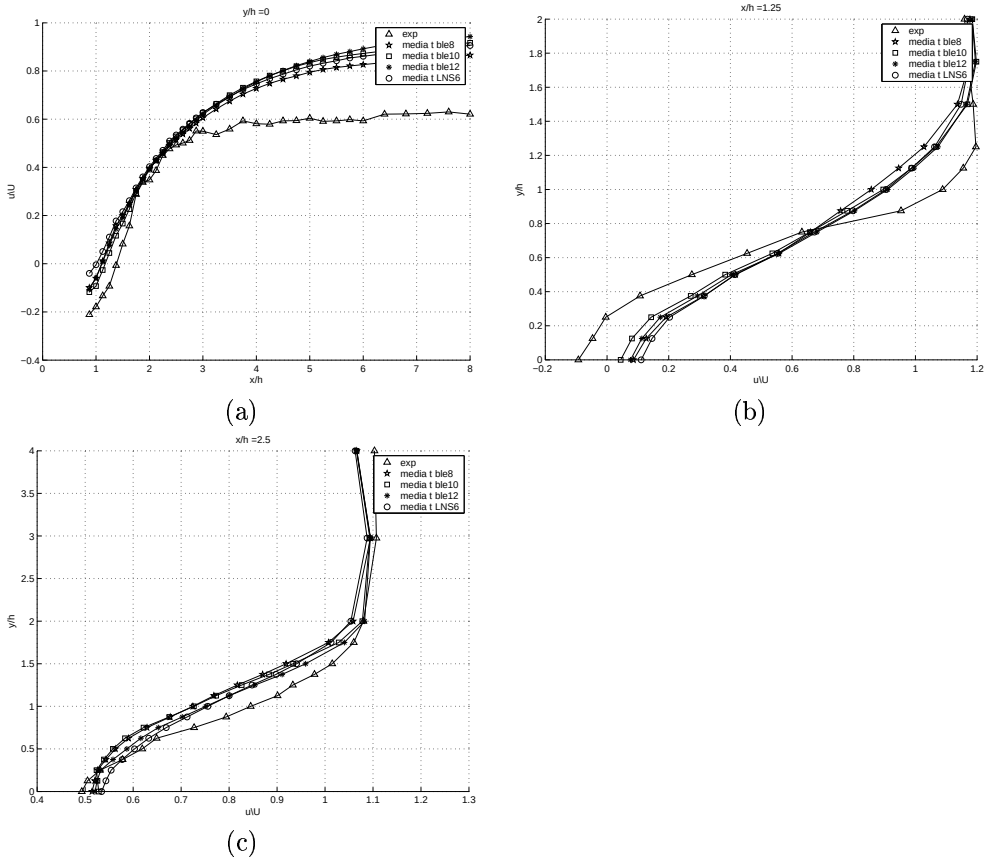

Figure 20: u velocity profiles for BLE8, BLE10, BLE12, LNS6 plane y/L=0 (a), x/L=1.25 (b), x/L=2.5 (c)

7 Conclusions

A new strategy for blending RANS and LES approaches into an hybrid model has been proposed, which is based on a decomposition of the flow variables in a RANS part (i.e. the averaged flow field), a correction part that takes into account the large turbulent scale fluctuations, and a third part made of the unresolved or SGS fluctuations. The RANS flow field is solved and, where the grid is adequately refined, it is corrected by adding the resolved turbulent fluctuations. This is done by means of a blending function, which assures that the model may coincide with the RANS approach where the grid is coarse and tends with continuity to the LES model as the grid is locally refined.

The proposed strategy is applied for blending the standard RANS $k-\varepsilon$ closure and the VMS-LES model with the Smagorinky closure. To this purpose, three different definitions of the blending function are proposed. The resulting hybrid RANS/VMS-LES method has been applied to the numerical simulation of a classical benchmark for bluff-body flows, i.e. the flow around an infinite-length square cylinder at $Re = 22000$. For comparison, another hybrid model has been considered here, obtained by applying the LNS blending criterion, which is based on the ratio between the RANS and the LES viscosity, to blend the standard RANS $k-\varepsilon$ closure and the Smagorinsky model.

The numerical discretization is based on a second-order accurate mixed finite-element/finite-volume method, applied to unstructured tetrahedral grids. It uses a sophisticated MUSCL reconstruction leading to a numerical viscosity made of sixth-order spatial derivatives. Either an explicit Runge-Kutta algorithm or a second-order time-accurate implicit scheme can be used to advance the equations in time.

Simulations have been carried out on two grid with different spatial resolution; sensitivity of the results to the inlet turbulent kinetic energy and to the parameter δ in the approximate wall treatment have been also appraised.

For the tests carried out with the more refined grid it has been shown that the results of the new hybrid model are in accord with those computed with LNS and the agreement with experimental data is acceptable. Also in the coarser grid the LNS and the new hybrid model give comparable results, and the agreement with the experimental data is not completely satisfactory even if, as shown in [7], comparable to that of other LES simulations in the literature.

The selected test case does not allow to highlight the sensitivity of the results to the different definitions of the blending function. This might be due to the fact that, in the considered flow, separation is fixed by the geometry and this might reduce the sensitivity of the results to the different choices in the turbulence model. Consequently, new test cases should also be considered for further testing the different blending functions as, for instance, the flow around a circular cylinder which is a challenging and widely studied flow. However, from an a-posteriori analysis on the proposed blending functions it is shown that, although empirically based, they lead to a sensible behavior, at least for the present test-case. Indeed, for all the grid resolutions, the new hybrid model works in LES mode in the separated unsteady wake, and this is consistent with the rationale of hybrid models.

It is finally shown that the sensitivity of the results to the inlet turbulent kinetic energy is low. This means that the proposed hybrid model counterbalances the potential negative effect on the results that could be generated by the inaccurate prescription of the inflow turbulent kinetic energy. Conversely, it is shown that results are strongly affected by the parameter δ in the adopted wall-law, which consequently deserves a particular attention and a further investigation.

References

[1] P. Batten, U. Goldberg and S. Chakravarthy, *Interfacing statistical turbulence closures with large-eddy simulation*, AIAA Journal, 42(3), (2004).

[2] P.W. Bearman and E.D. Obasaju, *An experimental study of pressure fluctuations on fixed and oscillating square-section cylinders*, J. Fluid Mech., 119, (1982).

[3] G. Bosh and W. Rodi, *Simulation of vortex shedding past a square cylinder with different turbulence models*, Int. J. Num. Meth. Fluids, 28, (1998).

[4] S. Camarri, B. Koobus, M. V. Salvetti and A. Dervieux , *A low diffusion MUSCL scheme for LES on unstructured grids*, Technical Report RR-4512, INRIA, (2002).

[5] S. Camarri, B. Koobus, M. V. Salvetti and A. Dervieux , *Large-Eddy simulation of a bluff-body flow on unstructured grids*, Int. J. Num. Meth. Fluids, 40, (2002).

[6] S. Camarri, M. V. Salvetti, B. Koobus and A. Dervieux , *A low diffusion MUSCL scheme for LES on unstructured grids*, Computers and Fluids, 33, (2004).

[7] S. Camarri, M. V. Salvetti, B. Koobus and A. Dervieux , *Hybrid RANS/LES simulations of a bluff-body flow*, Wind and Structures, 8, (2005).

[8] C. Farhat, B. Koobus and H. Tran, *Simulation of vortex shedding dominated flows past rigid and flexible structures*, In Computational Methods for Fluid-Structure Interaction, Tapir, (1999).

[9] H. Guillard and C. Viozat , *On the behaviour of upwind schemes in the low Mach number limit*, Computers and Fluids, 28, (1999).

[10] J. Hinze, *Turbulence*, MacGraw-Hill, New York, (1959).

[11] T.J.R. Hughes, L. Mazzei and K.E. Jansen. *Large eddy simulation and the variational multiscale method*, Comput. Vis. Sci., 3, (2000).

[12] B. Koobus and C. Farhat, *A variational multiscale method for the large eddy simulation of compressible turbulent flows on unstructured meshes-application to vortex shedding*, Comput. Methods Appl. Mech. Eng., 193, (2004).

[13] E. Labourasse and P. Sagaut. *Reconstruction of turbulent fluctuations using a hybrid RANS/LES approach*, J. Comp. Phys., 182, (2002).

[14] M.H. Lallemand, H. Steve and A. Dervieux. *Unstructured multigridding by volume agglomeration: current statuts*, Comput. Fluids, 21, (1992).

[15] B.E. Launder and D.B. Spalding, *The numerical computation of turbulent flows*, Comp. Meth. Appl. Mech. and Eng., 3, (1979).

[16] D.A. Lyn and W. Rodi, *The flapping shear layer formed by flow separation from the forward corner of a square cylinder*, J. Fluid Mech., 267, (1994).

[17] R. Martin and H. Guillard , *A second order defect correction scheme for unsteady problems*, Computers and Fluids, 25(1), (1996).

[18] B. Mohammadi and O. Pironeau , *Unsyteady separated turbulent flows computation with wall-laws and $k-\varepsilon$ model*, Comput. Method Appl., 148(3-4), (1997).

[19] B. Mohammadi and G. Medic , *A critical evaluation of the classic $k-\varepsilon$ model and wall-laws for unsteady flows over bluff bodies*, Int. J. Comp. Fluid. Dyn., 10(1), (1998).

[20] P. L. Roe, *Approximate Riemann solvers, parameters, vectors and difference schemes*, J. Comp. Phys., 43, (1981).

[21] J. Smagorinsky, *General circulation experiments with the primitive equations*, Monthly Weather Review, 91(3), (1963).

[22] P.R. Spalart, W.H. Jou, M. Strelets and S. Allamaras, *Comments on the feasibility of LES for wings and on a hybrid RANS/LES approach*,Advances in DNS/LES, Columbus, OH., (1997).

[23] J.L. Steger and R.F. Warming, *Flux vector splitting for the inviscid gas dynamic equations with applications to the finite difference methods*, J. Comp. Phys., 40(2), (1981).

[24] B. van Leer, *Towards the ultimate conservative scheme. IV: A new approach to numerical convection*, J. Comp. Phys., 23, (1977).

Unité de recherche INRIA Sophia Antipolis
2004, route des Lucioles - BP 93 - 06902 Sophia Antipolis Cedex (France)

Unité de recherche INRIA Futurs : Parc Club Orsay Université - ZAC des Vignes
4, rue Jacques Monod - 91893 ORSAY Cedex (France)
Unité de recherche INRIA Lorraine : LORIA, Technopôle de Nancy-Brabois - Campus scientifique
615, rue du Jardin Botanique - BP 101 - 54602 Villers-lès-Nancy Cedex (France)
Unité de recherche INRIA Rennes : IRISA, Campus universitaire de Beaulieu - 35042 Rennes Cedex (France)
Unité de recherche INRIA Rhône-Alpes : 655, avenue de l'Europe - 38334 Montbonnot Saint-Ismier (France)
Unité de recherche INRIA Rocquencourt : Domaine de Voluceau - Rocquencourt - BP 105 - 78153 Le Chesnay Cedex (France)

Éditeur
INRIA - Domaine de Voluceau - Rocquencourt, BP 105 - 78153 Le Chesnay Cedex (France)
http://www.inria.fr
ISSN 0249-6399